Regular Article

A numerical direct scattering method for the periodic sine-Gordon equation

Filip Novkoski[1,a] , **Eric Falcon**[1,b] , **Chi-Tuong Pham**[2,c]

[1] CNRS, MSC, UMR 7057, Université Paris Cité, 75013 Paris, France
[2] CNRS, LISN, UMR 9015, Université Paris-Saclay, 91405 Orsay, France

Abstract We propose a procedure for computing the direct scattering transform of the periodic sine-Gordon equation. This procedure, previously used within the periodic Korteweg–de Vries equation framework, is implemented for the case of the sine-Gordon equation and is validated numerically. In particular, we show that this algorithm works well with signals involving topological solitons, such as kink or anti-kink solitons, but also for non-topological solitons, such as breathers. It also has the ability to distinguish between these different solutions of the sine-Gordon equation within the complex plane of the eigenvalue spectrum of the scattering problem. The complex trace of the scattering matrix is made numerically accessible, and the influence of breathers on the latter is highlighted. Finally, periodic solutions of the sine-Gordon equation and their spectral signatures are explored in both the large-amplitude (cnoidal-like waves) and low-amplitude (radiative modes) limits.

1 Introduction

Solitons are encountered in various fields of physics, from condensed matter, optics to hydrodynamics [1–4]. It has also received considerable attention in applied mathematics, in particular, in the study of integrable systems [5, 6]. Advanced tools of the inverse scattering transform (IST) have significantly changed the theoretical view of soliton solutions of nonlinear partial differential equations (PDEs), such as Korteweg–de Vries (KdV) and nonlinear Schrödinger (NLS) equations [7]. It has also recently led to experimental applications in optics [8] and in hydrodynamic surface waves [9], such as the experimental synthesis of soliton gas [10] or Peregrine solitons [11].

The sine-Gordon (SG) equation admits a variety of different soliton solutions, such as topological solitons (in the form of kinks or anti-kinks), non-topological breathers (i.e., solutions oscillating in time and localized in space), or multisolitons. Sine-Gordon solitons have been experimentally evidenced in the canonical example of a chain of coupled pendulums [12], but also in Josephson tunnel junctions between superconductors [13], dislocations in crystals [2, 4], or in biological cellular structures [14].

The SG equation has been extensively studied in the context of the IST [15], and, in particular, the initial value problem can be solved using IST methods [6, 16]. The corresponding Lax pairs are well known [17], whereas the spectral theory behind the SG equation with periodic boundary conditions has been developed using Floquet theory [18].

Generally speaking, if an integrable equation admits soliton solutions, a specific complex value λ can be assigned to each of such solitons, thus fully characterizing the solution. The value λ is the solution of a linear eigenvalue problem related to the given integrable nonlinear PDE. For example, in the case of the KdV equation, the linear problem is related to the Schrödinger equation, $\psi_{xx} - (u - \lambda)\psi = 0$, of the field $\psi(x, t)$ with an unknown potential $u(x, t)$ coming from the solution of the KdV solution [19]. A critical property of integrable equations is isospectrality, meaning that the values of λ are constant in time. The direct scattering problem aims to seek the values of λ (independent of time) from a given initial condition $u(x, 0)$. For the KdV equation, the values of λ are purely real, whereas, for the focusing NLS and SG equations, λ can take also complex values as well. While on the infinite line, this eigenvalue is unique, as we will see, in the periodic case this corresponds to a band which is bounded by two values. Numerical simulations of the eigenvalue equations of the direct scattering in the sine-Gordon framework have been performed, as well as the IST by numerically solving the related nonlinear eigenvalue problem to achieve the soliton spectrum [20, 21]. Here, we apply a more general and straightforward method for the direct scattering problem since it comes down to a product of matrices. Such a method has been previously applied to the KdV equation [7], and used experimentally in the periodic KdV equation [22].

Filip Novkoski, Eric Falcon, Chi-Tuong Pham authors contributed equally to this work.

[a] e-mail: filip.novkoski@u-paris.fr

[b] e-mail: eric.falcon@u-paris.fr

[c] e-mail: chi-tuong.pham@upsaclay.fr (corresponding author)

While SG solitons have been experimentally observed in various fields [12–14], a direct link between the direct scattering method and experimental data is still elusive so far. An experimental investigation of the integrability of physical systems described by the SG equation is yet to be made and would also provide a step towards the experimental study of integrable turbulence, in particular in the case of topological solitons, and for the synthesis of the corresponding soliton gas. Here, we present a tool and a case study of individual solutions to the SG equation, that could potentially allow for easy use of the direct scattering method on experimental data.

The article is organized as follows: in Sect. 2, we compare classic solutions of the SG equation on the real line to those satisfying periodic boundary conditions. In Sect. 3, we recall the scattering theory generally used in the literature and introduce a simpler numerical scattering method. We then apply the latter to well-known solutions and test its validity (Sect. 4 for one- and two-kink solitons, along with breathers; Sect. 5 for periodic trains of kinks and radiative modes). We draw our conclusions in Sect. 6.

2 The sine-Gordon equation on the real line and with periodic boundary conditions

2.1 On the real line

The (1+1) sine-Gordon equation (1 dimension of space and 1 of time) on the real line as an initial-value problem and for the unknown field $\phi(x, t)$, reads in nondimensional form

$$\phi_{tt} - \phi_{xx} + \sin \phi = 0, \tag{1}$$

for $(x, t) \in \mathbb{R} \times [0, \infty]$ and an initial condition $\phi(x, t = 0) = \phi_0(x)$.

One set of spatial boundary conditions can be chosen as "vanishing" ones at infinity, that is

$$\phi(x, t) \to 0 \quad (\mathrm{mod}\ 2\pi), \quad \text{as } |x| \to \infty \tag{2}$$

$$\phi_x(x, t) \to 0, \quad \text{as } |x| \to \infty. \tag{3}$$

In this article, we will refer to this SG equation along the real line, with vanishing boundary conditions as the iSG equation.

A well-known solitonic solution of this problem reads

$$\phi_{\mathrm{kink}}^{\sigma}(x, t) = 4 \arctan \exp\left[\sigma \frac{x - vt - x_0}{\sqrt{1 - v^2}}\right]. \tag{4}$$

The case $\sigma = +1$ corresponds to the so-called kink solution, whereas the case $\sigma = -1$ corresponds to the so-called anti-kink solution, both moving at speed $v \in\ ]-1, +1[$.

Note that throughout the rest of the article, we will refer to the term kink (resp. anti-kink) as a topological state connecting values of the function $\phi(x, t)$ going from $2n\pi$ to $2(n + 1)\pi$ (resp. $2m\pi$ to $2(m - 1)\pi$) as x increases, with m, n integers.

If the vanishing boundary conditions (2, 3) are disregarded, another set of solutions, moving at speed $v \in\ ]-1, +1[$, can be found as an infinite periodic train of kinks ($\sigma = +1$) or anti-kinks ($\sigma = -1$). They read

$$\phi_{\mathrm{am}}^{\sigma}(x, t) = \pi + \sigma\ \mathrm{am}\left(\frac{x - vt - x_0}{\sqrt{m(1 - v^2)}}, m\right), \tag{5}$$

where $\mathrm{am}(x, m)$ is the Jacobi amplitude function, for $m \in\ ]0, +1[$. They form a two-parameter family of solutions, parameterized by their speed v and the elliptic parameter m. $\sigma = +1$ is related to the increasing solution (kinks), whereas $\sigma = -1$ corresponds to the decreasing one (anti-kinks). Note that the limit-case $m = 1$ corresponds to the kink or the anti-kink solutions given by (4).

For such a solution, the spatial period Λ between two neighboring periodic kinks is given by

$$\Lambda(m, v) = 2\sqrt{m(1 - v^2)}\,\mathrm{K}(m), \tag{6}$$

where K is the complete elliptic function of the first kind.

2.2 Periodic boundary conditions

In the rest of the article, we study the (1+1) SG equation (1) but we impose "periodic" boundary conditions with a spatial period L:

$$\phi(x + L, t) = \phi(x, t) \quad (\mathrm{mod}\ 2\pi), \tag{7}$$

$$\phi_x(x + L, t) = \phi_x(x, t), \tag{8}$$

We assume that the initial condition $\phi(x, t = 0) = u(x)$, as well as $\phi_x(x, t = 0)$ and $\phi_t(t = 0)$ are known. We will call this set of equations the periodic sine-Gordon equation (pSG). The classic sine-Gordon equation is known as the continuous limit of a discrete

Fig. 1 Scheme in the complex plane of the energies, $E = \lambda^2$, of different types of soliton that can take real (topological soliton in red) or complex (breather soliton in blue) values
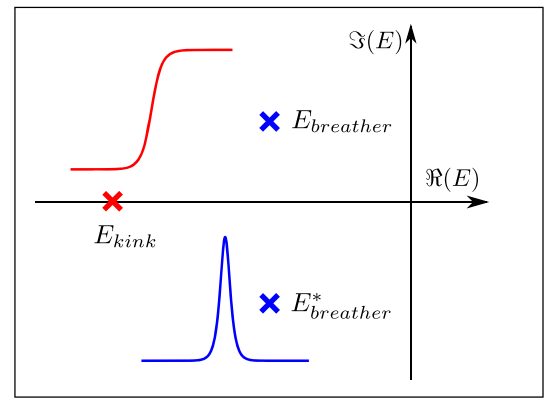
mechanical chain of torsionnally coupled pendula. Here, the periodic conditions (7, 8) turns the usual straight pendulum chain into a circle chain and includes possible non-zero topological charges, hence the possible presence of kinks.

The length L will be chosen to be larger than the typical length scale equal to 1 in the case of the nondimensional SG equation (1).

The equivalent of the 1-kink solution for such periodic boundary conditions and moving at speed v corresponds to the solution given by (5), provided the distance between two successive periodic kinks is L, namely we have the relationship between L, v, m

$$L = \Lambda(m, v) = 2\sqrt{m(1 - v^2)}\, \mathrm{K}(m). \tag{9}$$

In turn, the N-periodic kink solutions (in the sense of a $2N\pi$-jump in ϕ) for such periodic boundary conditions are given by (5), with the relationship between L, v, m, N

$$L = N\Lambda(m, v) = 2N\sqrt{m(1 - v^2)}\, \mathrm{K}(m). \tag{10}$$

3 Direct scattering method

From the solutions of the pSG equation, we wish to obtain the nonlinear spectral content of our system. To that end, the SG equation is viewed as a compatibility condition of two matrix equations [15]

$$\Psi_x = \mathrm{i}\left[\frac{\lambda}{2}\boldsymbol{\sigma}_z + \frac{\phi_x - \phi_t}{4}\boldsymbol{\sigma}_x - \frac{\boldsymbol{\sigma}_z \cos\phi + \boldsymbol{\sigma}_y \sin\phi}{8\lambda}\right]\Psi,$$
$$\mathrm{i}\Psi_t = \left[\frac{\lambda}{2}\boldsymbol{\sigma}_z + \frac{\phi_x - \phi_t}{4}\boldsymbol{\sigma}_x + \frac{\boldsymbol{\sigma}_z \cos\phi + \boldsymbol{\sigma}_y \sin\phi}{8\lambda}\right]\Psi, \tag{11}$$

where $\Psi(x, t)$ is a two-component complex Jost function, and $\boldsymbol{\sigma}_j$ are the Pauli matrices with $j = x, y$ or z

$$\boldsymbol{\sigma}_x = \begin{bmatrix} 0 & +1 \\ -1 & 0 \end{bmatrix}; \boldsymbol{\sigma}_y = \begin{bmatrix} 0 & -\mathrm{i} \\ +\mathrm{i} & 0 \end{bmatrix}; \boldsymbol{\sigma}_z = \begin{bmatrix} +1 & 0 \\ 0 & -1 \end{bmatrix}. \tag{12}$$

Unlike the KdV or NLS equation, where the problem of finding λ is essentially linear, here we are dealing with an eigenvalue problem which is linear in Ψ but nonlinear in λ. We will be interested in finding the value E, which we refer to as *energy*, such that $\lambda = \sqrt{E}$.

Because of the periodic boundary conditions, it is possible to gain more insight of the problem by applying Floquet theory [18]. After fixing a given point x_0, we consider a basis of solutions $\{\Psi_+(x, x_0, E), \Psi_-(x, x_0, E)\}$ such that

$$\Psi_+(x = x_0, x_0, E) = \begin{bmatrix} 1 \\ 0 \end{bmatrix}, \tag{13}$$

$$\Psi_-(x = x_0, x_0, E) = \begin{bmatrix} 0 \\ 1 \end{bmatrix}. \tag{14}$$

Due to the periodicity, the functions $\Psi_+(x + L, x_0, E)$ also have to be solutions of Eq. (11), and are expressible in terms of the basis functions. This leads us to write

$$\begin{bmatrix} \Psi_+(x + L, x_0, E) \\ \Psi_-(x + L, x_0, E) \end{bmatrix} = \mathbf{S}(E)\begin{bmatrix} \Psi_+(x, x_0, E) \\ \Psi_-(x, x_0, E) \end{bmatrix} \tag{15}$$

where $\mathbf{S}$ is the scattering matrix (or transfer matrix, also called the *monodromy matrix*). In order for the solutions to be bounded, certain conditions need to be imposed onto the matrix. In addition, the spectrum of the problem in Eq. (11) is divided into its *discrete* and *continuous* parts.

The eigenvalues of the discrete spectrum correspond to solitons and are such that they satisfy [18]

$$|\operatorname{tr}(\mathbf{S})| = 2, \tag{16}$$

$$\Im(\operatorname{tr}\mathbf{S}) = 0, \tag{17}$$

where $\Im$ stands for the imaginary part. In addition, for real potentials, the eigenvalues are negative. Thus, the solitons will lie in the $E < 0$ plane as shown in Fig. 1, for the case of kinks (for which $E \in \mathbb{R}$) and breathers ($E \in \mathbb{C}\backslash\mathbb{R}$).

On the other hand, the continuous spectrum consists of eigenvalues such that $E > 0$ with

$$|\operatorname{tr}(\mathbf{S})| \leq 2, \tag{18}$$

$$\Im(\operatorname{tr}\mathbf{S}) = 0. \tag{19}$$

This part of the spectrum is associated with the radiation of phonons, i.e., the dispersive component of the wave field. Thus, in order to spectrally detect the solitons (in the E-plane), numerical computations of the trace of the monodromy matrix are needed.

In this article, we tackle the problem by following a different approach, using a method similar to that first used in Refs. [7, 23] for the periodic KdV case. Expanding the Jost function at $x + \Delta x$ yields

$$\Psi(x + \Delta x) = e^{\mathbf{T}\Delta x}\Psi(x) = \mathbf{Q}(x)\Psi(x), \tag{20}$$

where the matrix $\mathbf{T}$ is inferred from Eq. (11) and $\mathbf{Q}$ is defined as $\mathbf{Q}(x) \equiv e^{\mathbf{T}\Delta x}$. By iterating the above process over a piecewise constant signal containing N points, we find the scattering matrix

$$\mathbf{M}(E) = \prod_{n=N-1}^{0} \mathbf{Q}(x_n, E), \tag{21}$$

which relates now $\Psi(x + L)$ to $\Psi(x)$, with $x_n = n\Delta x$ and $\Delta x = L/N$. By choosing $x = x_0$, we have $\operatorname{tr}(\mathbf{M}) = \operatorname{tr}(\mathbf{S})$. Note that our calculation of $\mathbf{M}(E)$ consists in a mere product of matrices, whereas the computations of $\mathbf{S}(E)$ is based on non-straightforward numerical schemes [20].

In order to simplify computations, we are able to reduce the matrix $\mathbf{Q}$ of Eq. (20) to

$$\mathbf{Q} = \cos(\Delta x)\mathbb{I} + i\sin(\Delta x)\vec{\mathbf{v}} \cdot \vec{\boldsymbol{\sigma}}, \tag{22}$$

$$\text{with} \quad \vec{\mathbf{v}} = \left(\frac{\phi_x - \phi_t}{4}, -\frac{\sin\phi}{8\lambda}, \frac{\lambda}{2} - \frac{\cos\phi}{8\lambda} \right), \tag{23}$$

speeding calculations up around two times. In practice, in order to compute $\mathbf{Q}$, we assume that $\phi(x, t = t_0)$ as well as $\phi(x, t = t_0 + \Delta t)$ are known, since one only has to have information of the time derivative at t_0. Knowing the full temporal evolution of ϕ is unnecessary. Despite this simplification, computation using complex values is still required. A decomposition of Eq. (21) into real and imaginary parts would be a further improvement, but is not obvious.

In the following, using well-known solutions along with their spectral characteristics, we will test this numerical method and compare its results to those of the literature (for instance those studied in Ref. [18] using the $\mathbf{S}$ matrix).

4 One- and two-soliton solutions

4.1 Single kink solitons for periodic boundary conditions

Let us begin with the topological soliton solutions of the pSG equation, i.e, periodic kinks and anti-kinks (see Eqs. (5) and (9)). We examine three solitons, with the same velocity $v = 0.3$, but different values of the elliptic parameter $m = 0.5, 0.8, 0.99$, described by Eq. (5). Using the algorithm prescribed above, based on the calculation of the matrix $\mathbf{M}(E)$, we use these three soliton solutions to compute their corresponding traces of the scattering matrix. We focus on kinks, i.e. $\sigma = +1$, and the space domain is chosen so that it corresponds to one period leading to one single soliton. As a consequence, each spatial domain has a different length L.

The results for the traces are shown in Fig. 2. We observe that for all those three solitons, there is one intersection with $+1$ and one with -1 as expected theoretically. These intersections corresponding to solitons, we see that the method permits their detection. As the elliptic parameter is varied, the two corresponding energies move closer and closer together (and in the limit of $m = 1$, they would coincide). The velocity v and elliptic parameter m are linked to the energies of the soliton and are given by

$$m = \frac{2}{1 + \frac{1}{2}\left[\sqrt{E_2/E_1} + \sqrt{E_1/E_2}\right]}, \tag{24}$$

Fig. 2 Half-trace of the monodromy matrix $\mathbf{M}(E)$ for three kink solitons with periodic boundary conditions, $m = 0.5$, 0.8, 0.99. The trace crosses the lines ± 1 only once respectively for all three. We observe how the energies move closer together as m moves towards 1. Inset: Single kink waveform $\phi(x, 0) = u(x)$ given by Eq. (5) and used as the initial condition for the direct scattering method with $m = 0.8$ and $m = 0.99$ (same color as in the main figure). Note that, in both cases, we have used three periods $L(m)$ (see Eq. (9)) as an illustration of their periodicity (hence a 6π-jump)
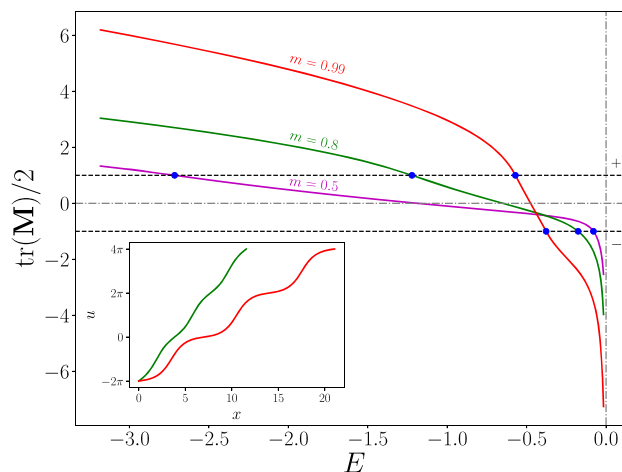
Fig. 3 Half-trace of the monodromy matrix $\mathbf{M}(E)$ for a kink soliton. Only one crossing of the trace at ± 1 is found for a negative value of the energy, $E = -1$, as expected theoretically. Inset: The kink-soliton waveform $\phi(x, 0) = u(x)$ used as the initial condition for the direct scattering method (Eq. (4), with $L = 20$)
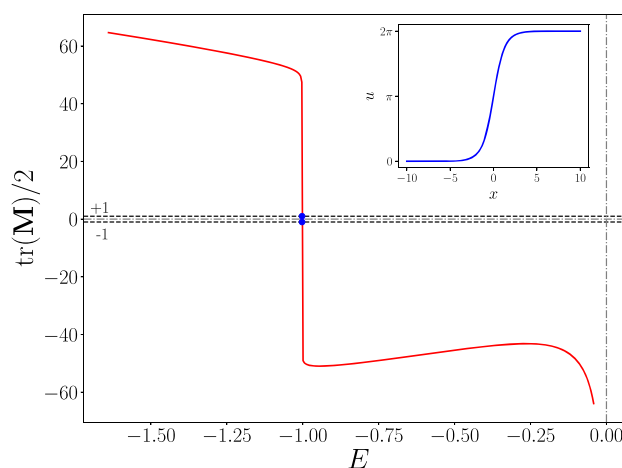
$$v = \frac{4(E_1 E_2)^{1/2} - 1}{4(E_1 E_2)^{1/2} + 1}, \tag{25}$$

as computed using expressions found in [18]. It is worth mentioning that previous references dealing with this type of solutions do not state that the elliptic parameter m is fixed by the energies in this way. Using a bisection method, we numerically determine the intersections with $\mathrm{tr}(\mathbf{M})/2 = \pm 1$, allowing us to obtain the energies E_1 and E_2. Given this statement, along with Eq. (24), we are able to confirm that the method correctly identifies the solitons, with the numerical error being within 0.3%.

4.2 Truncated kink soliton of the whole line

Here, we will truncate the kink solution on the real line. We want to show in what extent the numerical procedure still holds when the input signal is not an exact solution (here, the boundary conditions (Eqs. (7) and (8)) are not satisfied). Let us begin with the topological soliton solutions of the iSG equation, i.e, kinks and anti-kinks.

A single soliton solution with energy $E = -K$ is given by (4) and its velocity v satisfies

$$v = \frac{4K - \sigma}{1 + 4K\sigma}, \tag{26}$$

for $\sigma = \pm 1$ discriminating kinks (+) from anti-kinks (−) [24].

We apply the algorithm proposed in Sect. 3 in order to compute the trace of the scattering matrix $\mathbf{M}$ and to find the eigenvalues λ of the following signal. The input signal is chosen to be a kink (displayed in the inset of Fig. 3), for which we take $K = 1$ in Eq. (26), $\sigma = +1$, and $u(x) = \phi(x, 0)$ as in Eq. (4) consisting of $N = 1000$ points, on an interval of length $L = 20$. While the signal is a solution for the infinite line, and does not satisfy perfectly the periodic boundary condition, we consider that the errors due to the mismatch at the two ends will be negligible and use the given form of the field nevertheless. By iterating over both the signal and different values for the energy E, we find the half-trace of the matrix $\mathbf{M}(E)$ as shown in Fig. 3. The imaginary part of the trace is zero, and the real part of $\mathrm{tr}(\mathbf{M})/2$ takes values ± 1 at $E_1 = E_2 = -1.0024$, as expected. These values of the crossings

Fig. 4 Half-trace $\mathbf{M}(E)$ for a pair of kink solitons with different energies. As predicted theoretically, two crossings at the negative energies are found, corresponding numerically well to those prescribed. $L = 100$. Inset: Signal used as the initial condition $u(x)$ in the direct scattering, with energies $E = -1$ and $E = -1.5$ (see Eq. (27))
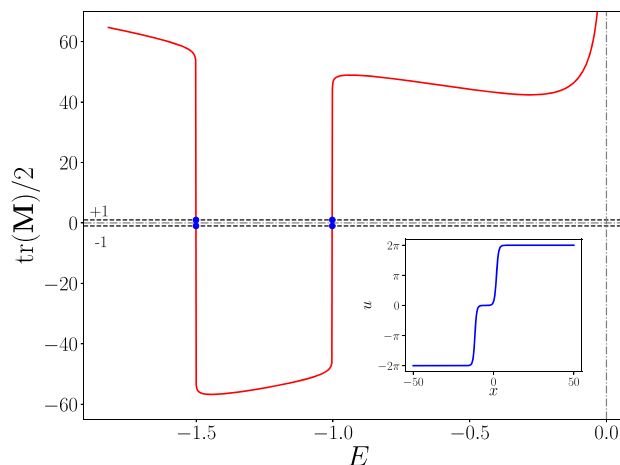
are obtained using the bisection method with the cutoff precision set to 10^{-12}. We do not notice a numerical difference between the two values. Close to $E = 0$ the trace tends to $-\infty$ which is expected theoretically [18]. In conclusion, the algorithm has detected the presence of a kink soliton on a line, without imposition of periodic boundary conditions.

4.3 Two-kink solution

We apply now the procedure for a signal consisting of a pair of two kinks with two different energies K_1 and K_2 and their corresponding velocities v_1 and v_2. The input signal is calculated using the formula for a two-kink solution that can be obtained through a Bäcklund transform [25] and reads

$$u(x,t) = 4 \arctan\left(k \frac{\phi_1 - \phi_2}{1 + \frac{\phi_1}{\phi_2}} \right), \tag{27}$$

$$\phi_j = \exp\left(\frac{x - v_j t}{\sqrt{1 - v_j^2}} \right), \quad v_j = \frac{4K_j - 1}{1 + 4K_j}, \tag{28}$$

$$k = \frac{\beta_1 - \beta_2}{\beta_1 + \beta_2}, \quad \beta_j = \frac{1 - v_j}{1 + v_j}, \quad j = 1, 2. \tag{29}$$

We here stress that the link between the eigenvalues, i.e. K_1 and K_2, and the velocities (v_1 and v_2) is the same as for the one-kink solution. This link has not been clearly stated in the literature, to our knowledge.

The initial condition that we used is shown in the inset of Fig. 4 for $L = 100$, with the energies of the two solitons fixed at values $K_1 = 1$ and $K_2 = 1.5$. In response to this initial condition, the numerically computed half-trace $\mathbf{M}(E)$ is shown in Fig. 4. The energies found using the bisection method lead to $E_1 = E_2 = -1.5009$ and $E_3 = E_4 = -1.0024$, which is in excellent agreement with the prescribed initial soliton energies. The application of the algorithm to arbitrary numbers of kink or anti-kink solitons is thus achievable as long as their energies are different enough. Due to the fact that their energies are real numbers, the detection of kinks and anti-kinks is numerically easy, and the computation time is relatively short. The case of a kink train will be tested below in Sect. 5.
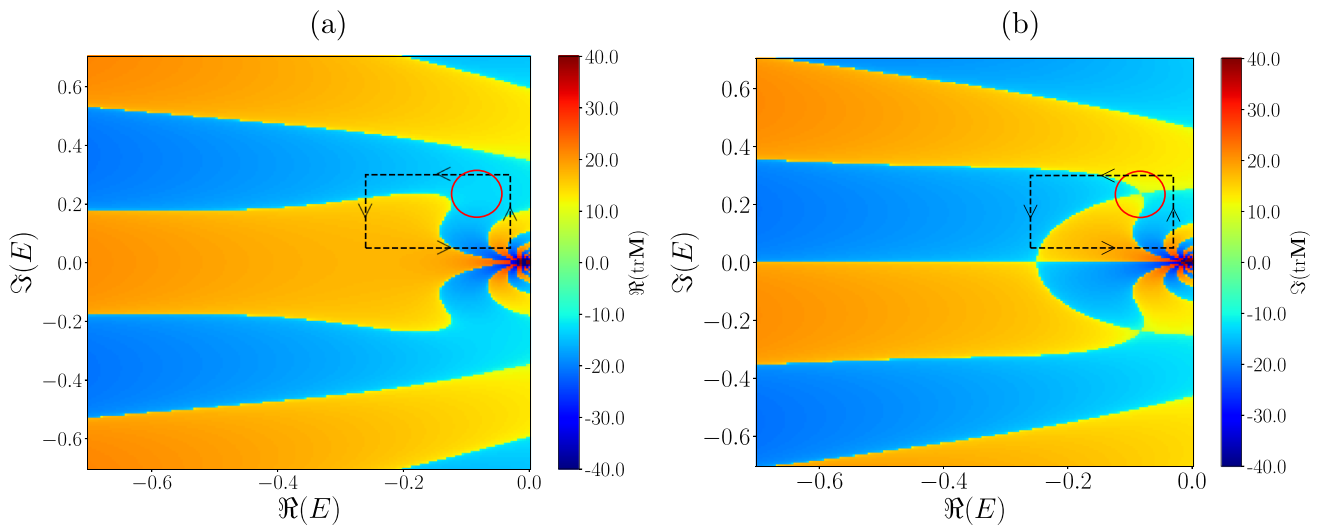
4.4 Breathers

The breather is a time-oscillating and spatially localized soliton of the SG equation which can be described by an angle $0 < \mu < \pi/2$ in the complex plane of λ and is associated with two complex values of $\lambda_{1,2} = \sqrt{E} = \pm \frac{1}{2} e^{\pm i\mu}$ [24]. Its shape is given by

$$\phi(x,t) = 4 \arctan\left[\tan\mu \frac{\sin(t \cos\mu + \phi_0)}{\cosh(x \sin\mu)} \right]. \tag{30}$$

Our calculation of the trace must be extended to complex values of the energy and we shall be looking for the points where $\Im(\text{tr}\,\mathbf{M}) = 0$ and still $\Re[\text{tr}\,(\mathbf{M})/2] = 1$. Nevertheless, we find that the presence of breathers is easily identified by simple inspection of the imaginary part of the trace, from which we numerically find and confirm their energies.

We take the value of $\mu = \pi/3$ and apply the algorithm to a single breather. The search for the eigenvalue is now extended into the complex plane by calculating the trace on a mesh of energies. The real part of the trace of $\mathbf{M}$ is shown in Fig. 5a, alongside the imaginary part in Fig. 5b. We observe an entangled pattern of values, which oscillate from positive to negative values. The focus should be put on the imaginary part of the trace, which gives a qualitative hint of the presence of a breather.

Fig. 5 a Real part of the trace of $\mathbf{M}(E)$ showing only a slight deformation close to the complex value of the breather energy. **b** Imaginary part of the trace of $\mathbf{M}(E)$ in the complex plane of energy E demonstrating a strong "pinch" close to the breather energy $E = \frac{1}{4}e^{2i\pi/3}$ (red circle)

Fig. 6 Real function $G(E)$ of Eq. (31) around the region of the breather energy. We observe clearly the appearance of a zero of the function at the value of the prescribed energy $E = -1/8 + \sqrt{3}i/8$
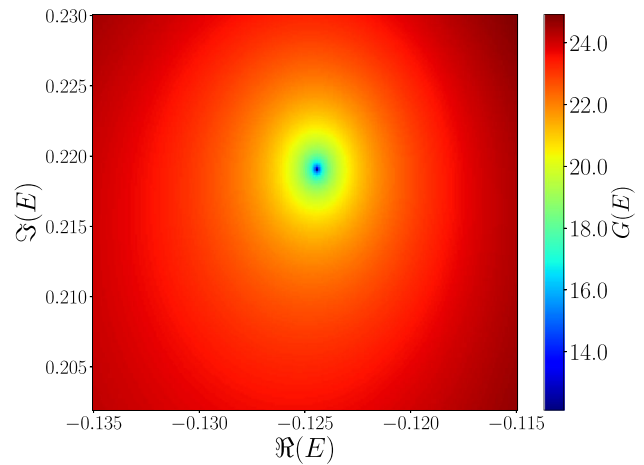
The breather changes the spectrum by "pinching" together two regions of negative (and positive) values of the imaginary part of the trace. Without the presence of the soliton, the regions are well separated and smooth (see Appendix A). The accurate location of the "pinch" in the E-space does not correspond exactly to its eigenvalue, and depends on the resolution of the mesh, but it serves as a good qualitative indicator.

In order to locate the exact position of the breather eigenvalue we use the pinch as a first guess, and focus on the function

$$G = \left[|\Re(\operatorname{tr}\mathbf{M})| - 2 \right]^2 + \left[\Im(\operatorname{tr}\mathbf{M}) \right]^2 \tag{31}$$

which will be identically zero when the real part is equal to 2 and the imaginary part is zero. We plot this function $G(E)$ in a zoomed-in region around the pinch in Fig. 6. As we can see, there is a single minimum, which corresponds to the breather eigenvalue. By applying a root-finding algorithm, we find the location of the root to be $E = -0.1268 + 0.2116i$, which up to our precision, is close to the expected value of $E = -\frac{1}{8} + \frac{\sqrt{3}}{8}i$. For the root-finding procedure, the position of the minimum found in Fig. 6 was taken as the initial guess.

In order to better quantify the detection of breathers instead of just relying on visual inspection, we use Cauchy's argument principle which states that

$$I = \frac{1}{2i\pi} \oint_\gamma \frac{f'(z)}{f(z)} \, \mathrm{d}z, \tag{32}$$

for a holomorphic function $f(z)$ and a closed contour γ, is an integer equal to Z, the number of zeros of f enclosed by γ and counted with their multiplicities. Here we compute the value of I with $f(z) = \operatorname{tr}\mathbf{M}(z) - 2$. For the sake of simplicity and efficiency, we use a regular Cartesian grid of point of the complex E-plane, a rectangle contour γ based on the grid points and centered differences
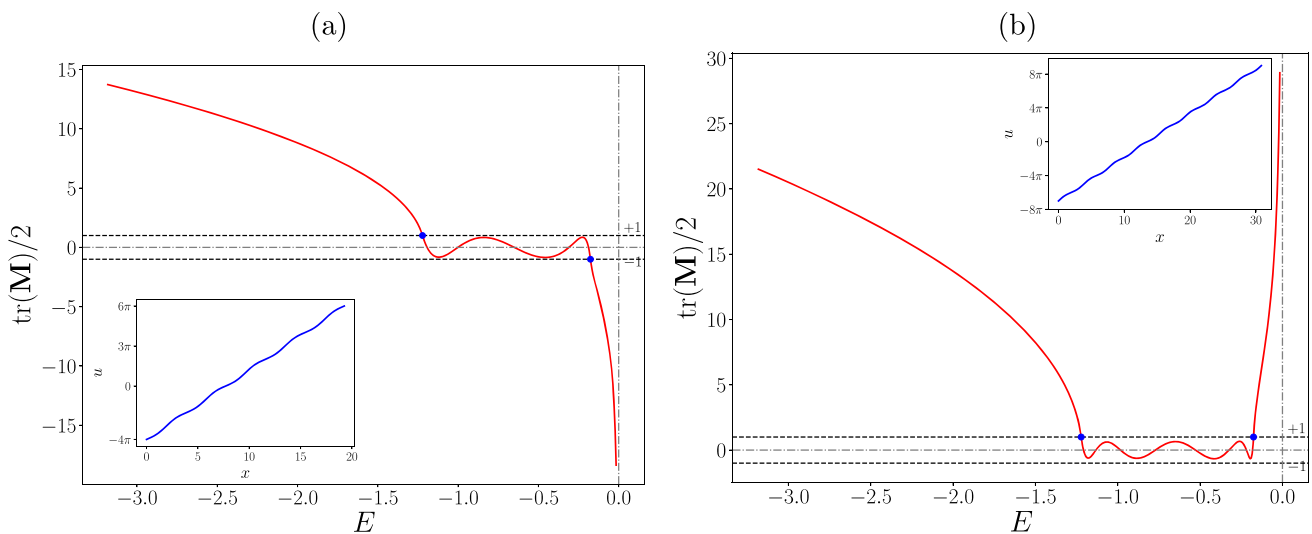
Fig. 7 Half-trace of the monodromy matrix **M** for a train of kinks (as in the initial condition in the inset), defined by two different energies. In addition to the crossings at the expected energies (blue dots), we observe that the trace is indeed zero between these two values. **a** Case of a train of $N = 5$ kinks, **b** Case of a train of $N = 8$ kinks. Depending on the parity of N, the value of the half-trace of the monodromy matrix **M** only crosses the value +1 of both the values +1 and −1

for the calculation of the complex derivatives along γ. We use the trapezoidal rule in order to compute the integral. The value of the index is found to be $I = 0.9995 \approx 1$ (the numerical error stemming from the discretization). It corresponds to one breather, since, much like the kink, the order of the zero of $\operatorname{tr}\mathbf{M} - 2$ is 1. This method has also been tested in the case of multiple breathers and found to be reliable: for instance, four breathers lead to $I = 4$, provided γ encloses the four zeros of f (data not shown).

5 Periodic solutions: trains of kinks and radiative modes

We now turn to the periodic solutions of the SG equation. We will be interested only in stable solutions [12]. We will first test the method for nonlinear periodic solutions (cnoidal-like waves as a periodic train of kinks) and then linear periodic solutions as radiative modes.

5.1 Periodic train of kinks

We begin with the monotonically increasing kink train, which is characterized by two energies $E_1 < E_2 < 0$, and requires that $(E_1 E_2)^{1/2} > 1$. Its form is given by Eq. (5), and the number of kinks that are contained in the domain sets the size of the latter through Eq. (10). The velocity v and elliptic parameter m are given by Eq. (24). If we let E_1 and E_2 approach each other, the distance between the kinks increases and we recover the single kink solution of Eq. (4).

In order to test our direct scattering method on this solution, let us choose the kink train velocity to be $v = 0.3$ and the elliptic parameter $m = 0.8$. The half-trace $\mathbf{M}(E)$ is shown in Fig. 7 for two cases of a N-soliton train. We clearly observe that the half-trace is equal to 1 at a low energy value E_1, then is equal to −1 at a higher energy value E_2 (Fig. 7a). Conversely, when N is even, the half-trace is equal to +1 at two energy values (Fig. 7b). In both cases, the numerically obtained values of the energies are found to be $E_1 = -1.2222$ and $E_2 = -0.1757$, giving $v = 0.2991$ and $m = 0.797$. Moreover, and more interestingly, we observe that the two eigenvalues are both located at the intersection with +1 for an even number of kinks, and that the value of the half-trace remains within ±1 between the two and oscillates $N - 1$ times. This is what distinguishes the kink train from the pure kink solution.
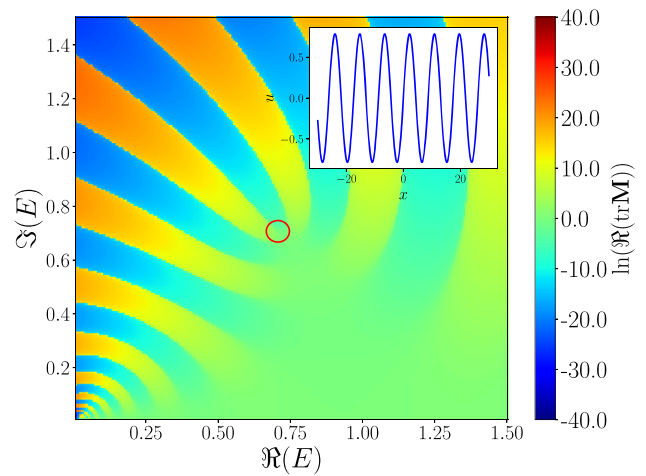
5.2 Radiative modes

Let us now turn to small-amplitude periodic solutions, which will illustrate the dispersive or radiative components of the spectrum. This solution is governed by two values of the energy $E_1 = E_2^* = |E_1| e^{i\alpha}$ located near the positive real axis [12, 18]. The form of the waves is given as

$$u = 2 \arcsin\left[\sqrt{m}\,\operatorname{sn}\left(\frac{x - vt}{\sqrt{1 - v^2}}, m\right)\right], \tag{33}$$

Fig. 8 Real part of the trace of **M** for an oscillatory radiation excitation, as described by Eq. (33). The presence of such a mode distorts the trace at positive values of the real part of the energy, especially close to the prescribed mode energy. Inset: Waveform of Eq. (33) used at $t = 0$. Logscale colorbar

Fig. 9 Value of the function $G(E)$ of Eq. (31). A zero of this function is found at the prescribed energy, as expected. We notice also additional zeros, corresponding to other radiative modes. Logscale colorbar
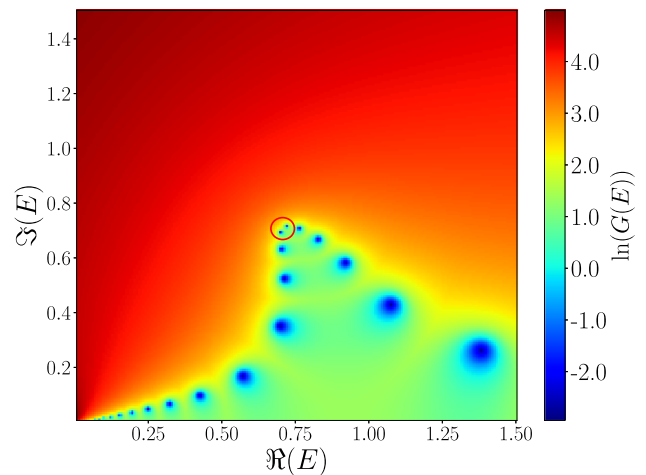
where $\text{sn}\,(x, m)$ is the Jacobi elliptic function of the first kind with elliptic parameter m. The velocity v and parameter m are slightly modified with respect to that of Eq. (24) and read

$$m = \sqrt{\frac{1 - \cos \alpha}{2}}, \tag{34}$$

$$v = \frac{1 + 4(E_1 E_2)^{1/2}}{1 - 4(E_1 E_2)^{1/2}}. \tag{35}$$

The amplitude of the wave is controlled through the angle of the energy α. We select a value of the energy with $\alpha = \pi/4$ and $|E_1| = 1$ and focus on the part of the complex plane with positive real values of $\text{tr}\,(\mathbf{M})$. The inset of Fig. 8 shows the waveform of Eq. (33) at $t = 0$. In Fig. 8, we only show the real part of the trace of the matrix **M** since there is no significant qualitative difference with its imaginary part. Similarly to the breather of Sect. 4, a distortion of the trace in the complex plane is observed, and a similar pinching is found close to the energy of the traveling kink-train, in particular when compared to the trace of **M** corresponding to a low-amplitude sine wave (see Appendix A). In order to evidence the presence of the prescribed energies in a clearer way, we once more make use of the function $G(E)$ of Eq. (31), which is plotted in Fig. 9. We clearly see that there is a zero at the position of the prescribed energy, circled in red, as predicted by Floquet theory. Other zeros, corresponding to similar radiative modes, are also present.

6 Conclusion

We have proposed a numerical method for the direct scattering problem of the periodic SG equation, based on a technique previously used in the case of the KdV equation. Applied to the SG equation, this method leads to obtaining the trace of the scattering matrix and finding the eigenvalues associated with the nontrivial direct scattering problem. We then computed the scattering matrix for several basic soliton solutions of the SG equation, for which the associated eigenvalues are either real (topological solitons as kinks,

anti-kinks, and kink trains) or complex in the energy complex plane in the case of non-topological solitons solutions (breathers) and periodic solutions.

This method avoids the direct and tedious solving of the nonlinear eigenvalue problem and can be easily applied to a given time series. This could potentially provide meaningful information in experiments, as in the cases of both the NLS and KdV equations. Furthermore, the dynamics of a large number of solitons, such as soliton gas, is a field of growing interest in the study of integrable turbulence [26], and the SG equation could provide richer dynamics with its topological soliton solutions.

Data Availability Statement No data associated in the manuscript.

Appendix A

As a comparison with the results on the different solitons and periodic solutions to the pSG equation discussed in the main text, we here include the half-trace obtained for a sine wave of amplitude $A = 0.01$, with $k = 2$ and $\omega = 1$ on a domain of length $L = 60$. The real and imaginary parts of the trace are shown in Fig. 10 for the negative real part of the energy plane, where we observe that there is no pinching. In Fig. 11 we show the same quantity for the positive real part of the energy plane.
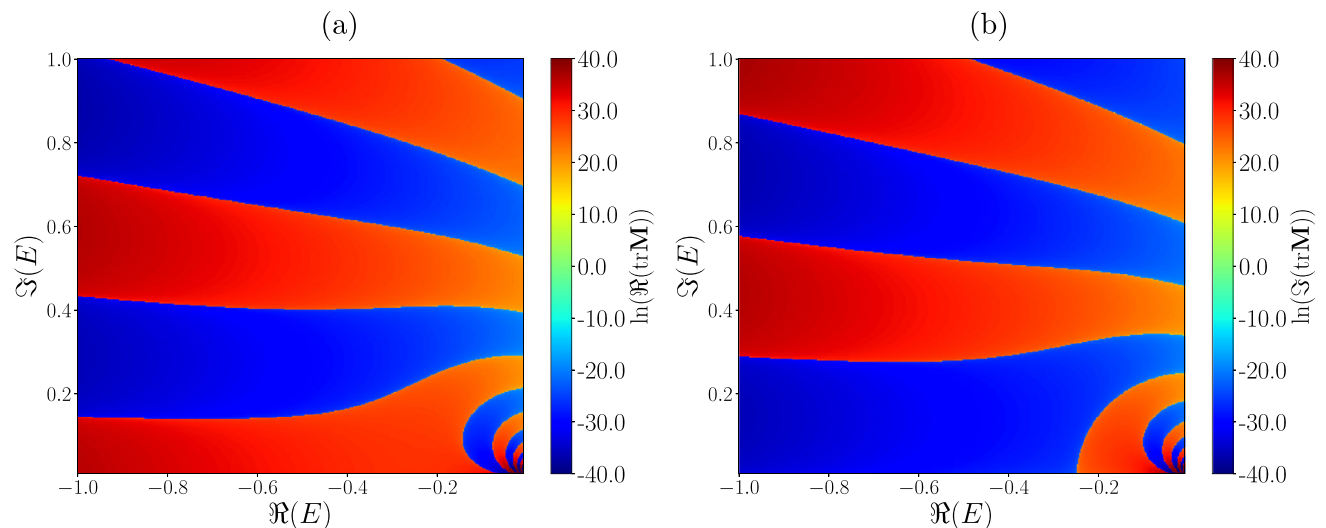

Fig. 10 a Real part of the trace of $\mathbf{M}(E)$ in the complex plane of energy, for negative $\Re(E)$, for a low-amplitude sine wave. **b** Imaginary part of the trace of $\mathbf{M}(E)$ for the same wave. Logscale colorbar
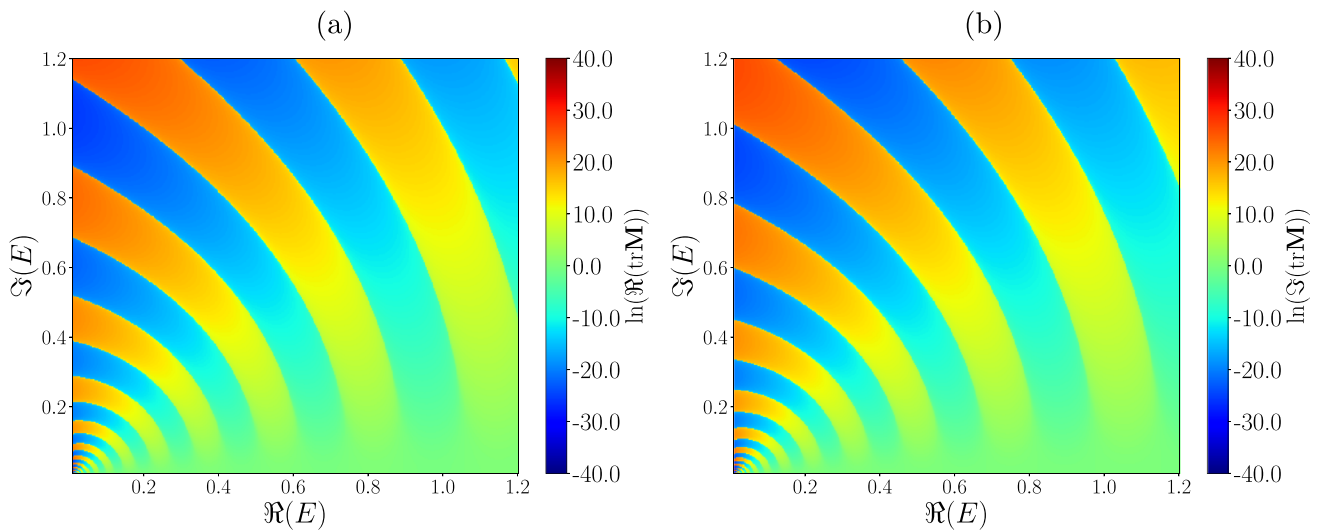
Fig. 11 a Real part of the trace of **M**(E) in the complex plane of energy, for positive $\Re(E)$, for a low-amplitude sine wave. **b** Imaginary part of the trace of **M**(E) for the same wave. Logscale colorbar

Appendix B

In this appendix, we discuss how the domain size L and the spatial discretization Δx affect the eigenvalues of a single infinite-line truncated kink soliton. We start varying L while keeping Δx fixed at 0.02. Its energy has been chosen to be $E = 1$. We can see in Fig. 12a that as the domain size L is increased, the results become more accurate. This is due to the fact that the errors due to periodicity (i.e. the mismatch at the domain ends) decreases. In Fig. 12b, we have kept the domain size value at $L = 20$ and changed the discretization Δx. As expected, by decreasing the value of Δx, the energies converge to a single value.
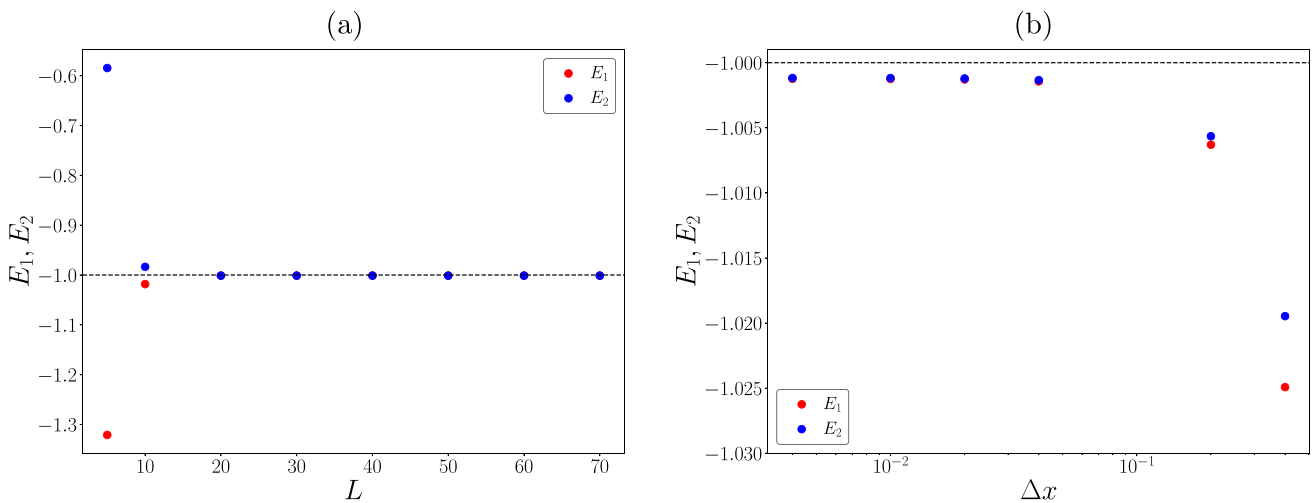
Fig. 12 a The eigenvalues of the truncated kink with energy $E = 1$ for different values of the domain size. **b** Eigenvalues of the truncated kink on a domain with fixed $L = 20$ for different values of the discretization Δx

References

1. J.S. Russell, Report on waves. Proc. R. Soc. Edinburgh **11**, 319 (1844)
2. J. Frenkel, T. Kontorova, On the theory of plastic deformation and twinning. Izv. Akad. Nauk Ser. Fiz. **1**, 137–149 (1939)
3. M. Remoissenet, *Waves Called Solitons*, 3rd edn. (Springer, Heidelberg, 1999)
4. T. Dauxois, M. Peyrard, *Physics of Solitons* (Cambridge University Press, Cambridge, 2006)
5. M.J. Ablowitz, H. Segur, *Solitons and the Inverse Scattering Transform* (Society for Industrial and Applied Mathematics, Philadelphia, 1981). https://doi.org/10.1137/1.9781611970883
6. P.G. Drazin, R.S. Johnson, *Solitons: An Introduction* (Cambridge University Press, Cambridge, 1989). https://doi.org/10.1017/CBO9781139172059
7. A.R. Osborne, *Nonlinear Ocean Waves and the Inverse Scattering Transform* (Academic Press, London, 2010)
8. P. Suret, M. Dufour, G. Roberti, G. El, F. Copie, S. Randoux, Soliton refraction by an optical soliton gas. Phys. Rev. Res. **5**, L042002 (2023). https://doi.org/10.1103/PhysRevResearch.5.L042002
9. I. Redor, E. Barthélemy, H. Michallet, M. Onorato, N. Mordant, Experimental evidence of a hydrodynamic soliton gas. Phys. Rev. Lett. **122**, 214502 (2019). https://doi.org/10.1103/PhysRevLett.122.214502
10. P. Suret, A. Tikan, F. Bonnefoy, F. Copie, G. Ducrozet, A. Gelash, G. Prabhudesai, G. Michel, A. Cazaubiel, E. Falcon, G. El, S. Randoux, Nonlinear spectral synthesis of soliton gas in deep-water surface gravity waves. Phys. Rev. Lett. **125**, 264101 (2020). https://doi.org/10.1103/PhysRevLett.125.264101
11. A. Tikan, F. Bonnefoy, G. Roberti, G. El, A. Tovbis, G. Ducrozet, A. Cazaubiel, G. Prabhudesai, G. Michel, F. Copie, E. Falcon, S. Randoux, P. Suret, Prediction and manipulation of hydrodynamic rogue waves via nonlinear spectral engineering. Phys. Rev. Fluids **7**, 054401 (2022). https://doi.org/10.1103/PhysRevFluids.7.054401
12. A.C. Scott, A nonlinear Klein–Gordon equation. Am. J. Phys. **37**(1), 52–61 (1969). https://doi.org/10.1119/1.1975404
13. A.V. Ustinov, Solitons in Josephson junctions. Phys. D **123**(1), 315–329 (1998). https://doi.org/10.1016/S0167-2789(98)00131-6
14. V.G. Ivancevic, T.T. Ivancevic, Sine-Gordon solitons, kinks and breathers as physical models of nonlinear excitations in living cellular structures. J. Geom. Symmetry Phys. **31**, 1–56 (2013). https://doi.org/10.7546/jgsp-31-2013-1-56
15. B.A. Malomed, In: Cuevas-Maraver, J., Kevrekidis, P.G., Williams, F. (eds.) The sine-Gordon Model: General Background, Physical Motivations, Inverse Scattering, and Solitons (Springer, Cham, 2014), pp. 1–30. https://doi.org/10.1007/978-3-319-06722-3_1
16. M.J. Ablowitz, D.J. Kaup, A.C. Newell, H. Segur, Method for solving the sine-Gordon equation. Phys. Rev. Lett. **30**, 1262–1264 (1973). https://doi.org/10.1103/PhysRevLett.30.1262
17. L.A. Takhtadzhyan, L.D. Faddeev, Essentially nonlinear one-dimensional model of classical field theory. Theoret. Math. Phys **21**, 160–174 (1974). https://doi.org/10.1007/BF01035551
18. M.G. Forest, D.W. McLaughlin, Spectral theory for the periodic sine-Gordon equation: A concrete viewpoint. J. Math. Phys. **23**(7), 1248–1277 (1982). https://doi.org/10.1063/1.525509
19. C.S. Gardner, J.M. Greene, M.D. Kruskal, R.M. Miura, Method for solving the Korteweg–de Vries equation. Phys. Rev. Lett. **19**, 1095–1097 (1967). https://doi.org/10.1103/PhysRevLett.19.1095
20. E.A. Overman II., D.W. McLaughlin, A.R. Bishop, Coherence and chaos in the driven damped sine-Gordon equation: Measurement of the soliton spectrum. Phys. D **19**(1), 1–41 (1986). https://doi.org/10.1016/0167-2789(86)90052-7
21. R. Flesch, M.G. Forest, A. Singha, Numerical inverse spectral transform for the periodic sine-Gordon equation: Theta function solutions and their linearized stability. Phys. D Nonlinear Phenom. **48**(1), 169–231 (1991). https://doi.org/10.1016/0167-2789(91)90058-H
22. F. Novkoski, C.-T. Pham, E. Falcon, Experimental observation of periodic Korteweg–de Vries solitons along a torus of fluid. Europhys. Lett. **139**(5), 53003 (2022). https://doi.org/10.1209/0295-5075/ac8a12
23. A.R. Osborne, Automatic algorithm for the numerical inverse scattering transform of the Korteweg–de Vries equation. Math. Comput. Simulat. **37**(4), 431–450 (1994). https://doi.org/10.1016/0378-4754(94)00029-8
24. Y.S. Kivshar, B.A. Malomed, Z. Fei, L. Vázquez, Creation of sine-Gordon solitons by a pulse force. Phys. Rev. B **43**, 1098–1109 (1991). https://doi.org/10.1103/PhysRevB.43.1098
25. A. Barone, F. Esposito, C.J. Magee, A.C. Scott, Theory and applications of the sine-Gordon equation. Riv. del Nuovo Cim. **1**(2), 227–267 (1971). https://doi.org/10.1007/BF02820622
26. P. Suret, S. Randoux, A. Gelash, D. Agafontsev, B. Doyon, G. El, Soliton gas: Theory, numerics and experiments. arXiv:2304.06541v1 (2023)